Conductive Transparent TiN_x/TiO_2 Hybrid Films Deposited on Plastics in Air Using Atmospheric Plasma Processing

*Siming Dong, Makoto Watanabe, and Reinhold H. Dauskardt**

The successful deposition of conductive transparent TiN_x/TiO_2 hybrid films on both polycarbonate and silicon substrates from a titanium ethoxide precursor is demonstrated in air using atmospheric plasma processing equipped with a high-temperature precursor delivery system. The hybrid film chemical composition, deposition rates, optical and electrical properties along with the adhesion energy to the polycarbonate substrate are investigated as a function of plasma power and plasma gas composition. The film is a hybrid of amorphous and crystalline rutile titanium oxide phases and amorphous titanium nitride that depend on the processing conditions. The visible transmittance increases from 71% to 83% with decreasing plasma power and increasing nitrogen content of the plasma gas. The film resistivity is in the range of ~8.5×10^1 to 2.4×10^5 ohm cm. The adhesion energy to the polycarbonate substrate varies from ~1.2 to 8.5 J/m^2 with increasing plasma power and decreasing plasma gas nitrogen content. Finally, annealing the film or introducing hydrogen to the primary plasma gas significantly affects the composition and decreases thin-film resistivity.

1. Introduction

Titanium nitride (TiN_x) films have broad applications in electric devices because of their high electric conductivity and chemical stability.[1–3] TiN_x has been widely studied as a protective coating due to its high hardness and high thermal stability related to its high melting point (>3000 °C).[4] Studies of TiN_x deposited on silicon, glass and metal substrates have all been reported although the deposition procedures require vacuum or inert gas environments and often high deposition temperatures (>400 °C).[5–7] While TiN_x films have the potential for low resistivity, they have not been widely applied in optoelectric devices due to their high visible light absorption which limits transparency.[8] However, another titanium compound, titanium oxide (TiO_2), is an abundant and cost-effective oxide with excellent optical transparency related to its large band gap (~3.2 eV).[9–11]

In the present study we explored the possibility of depositing hybrid film blends of TiN_x and TiO_2 on plastics in ambient air to achieve optimal combinations of optical transparency along with good electrical conductivity. We employed a versatile atmospheric plasma deposition process that enables film deposition on large and/or complex shape substrates without the need for vacuum or inert deposition environments.[12,13]

The precursor (titanium ethoxide, TTEO) employed had a high boiling point so we employed a high temperature precursor delivery system to volatilize the precursor in a helium carrier gas.[12] We deposited TiN_x/TiO_2 hybrid films on both polycarbonate (PC) and silicon substrates under different processing conditions by varying the plasma power and the nitrogen content of the plasma gas. These conditions along with annealing of the films were investigated and correlated with the film properties including the deposition rate, film composition, optical transmittance, electrical resistivity and the adhesion energy to the polycarbonate substrate. Before annealing, the resistivity of films as low as ~8.5×10^1 ohm cm was achieved. To reduce the oxygen and carbon content of the films we created a reducing plasma environment by introducing hydrogen gas (H_2) into the primary plasma gas supply. The introduction of hydrogen was effective in reducing the resistivity of the films. Finally, we demonstrated that annealing at elevated temperature of the films on the silicon substrates was effective in reducing the film resistivity to ~6.1×10^{-1} ohm cm.

2. Results and Discussion

2.1. Film Morphology and Deposition Rate

Hybrid TiN_x/TiO_2 films with thicknesses of 400–600 nm were successfully deposited by atmospheric plasma in ambient air on the PC and silicon substrates. A scanning electron microscopy (SEM) image of the TiN_x/TiO_2 film deposited on the PC substrate is shown in **Figure 1**. The film morphology exhibited nanometer-sized particles that subsequent X-ray diffraction (XRD) revealed to be combinations of amorphous and crystalline particles. The films exhibited good optical transparency as shown by the optical image showing ~80%

S. Dong, Prof. R. H. Dauskardt
Department of Materials Science and Engineering
Stanford University
Stanford, CA 94305–2205, USA
E-mail: dauskardt@stanford.edu
Dr. M. Watanabe
High Temperature Materials Unit
National Institute for Materials Science
Ibaraki 305–0047, Japan

DOI: 10.1002/adfm.201303038

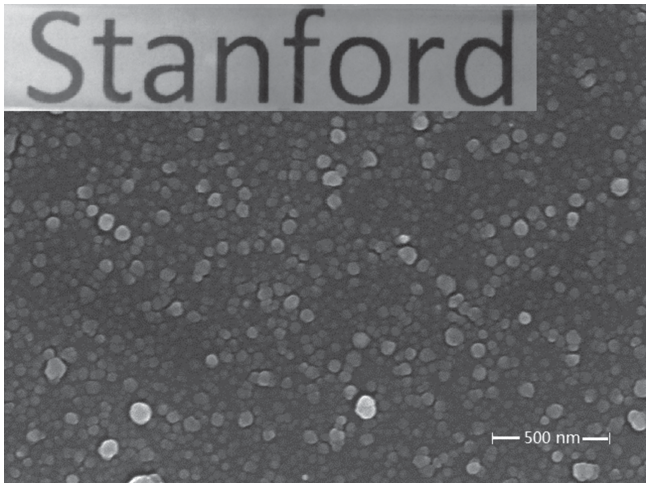

Figure 1. SEM image of and optical image of Atmospheric plasma deposition TiN_x/TiO_2 hybrid films on PC Substrate.

transmission through a ~500 nm film on a PC substrate (Figure 1 insert).

Average deposition rates R_d of the hybrid films grown on the PC substrates as a function of the plasma power and nitrogen flow rate are shown in **Figure 2**a and b. The deposition rate increased with increasing plasma power (60 W to 90 W) conforming to the expected trend that a higher plasma power generated a higher density of excited helium and nitrogen species to more effectively dissociate the precursor molecules (Figure 2a). This assumed that the nitrogen flow rate was kept constant and the amounts of precursor molecules delivered into the post- discharge region were the same for all deposition conditions. In Figure 2b the deposition rate was observed to decrease slightly with increasing nitrogen flow rate similar to the deposition rate trends reported for other plasma enhanced chemical vapor deposition (PECVD) processes.[14,15] The percentage of excited helium species decreased with increasing nitrogen flow rate since nitrogen has a higher electron affinity than helium and consumes more power during excitation.[14] In addition, excited nitrogen species also have a lower energy and shorter lifetime compared to excited helium species.[16] We therefore expect that the decomposition and resulting deposition rate of the precursor molecules will decrease with increasing nitrogen flow rate.

XRD studies of the hybrid TiN_x/TiO_2 films before and after annealing are shown in **Figure 3**. The films were deposited on silicon substrates to improve the fidelity of the XRD results and allow for the high temperature annealing. Before annealing, the hybrid film consisted of amorphous and crystalline TiO_2 rutile phase and amorphous TiN_x with no evidence of crystal TiN_x phase. To study the effect of annealing, films were deposited on silicon substrates with 90 W plasma power and 0.6 L/min N_2 flow rate. We annealed samples in N_2 for 4 h at 400 °C which is the temperature reported for the onset of TiN_x crystallization.[17] After annealing, the crystallinity of TiO_2 increased and crystal TiN_x cubic phase appeared (Figure 3).

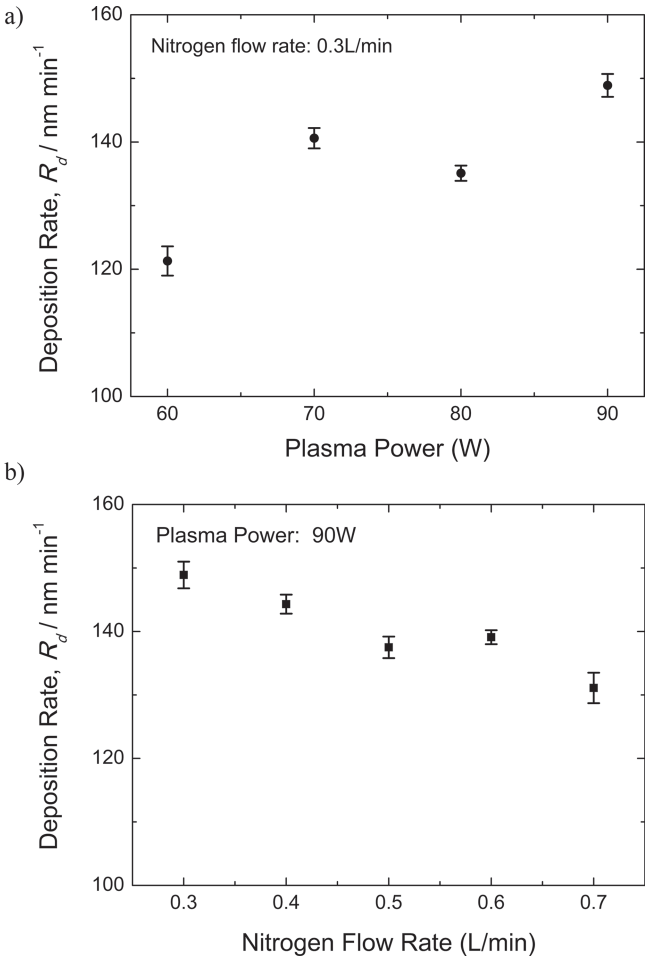

Figure 2. Variation of deposition rates of TiN_x/TiO_2 hybrid films on PC substrate as a function of a) plasma power b) nitrogen flow rate.

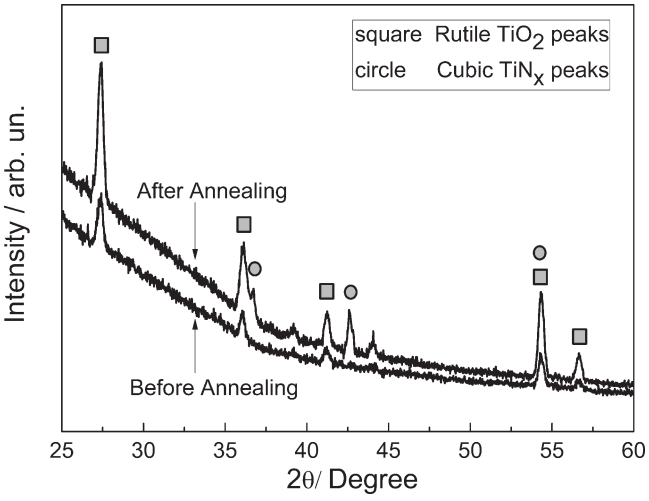

Figure 3. X-ray diffraction patterns of TiN_x/TiO_2 hybrid film before and after annealing.

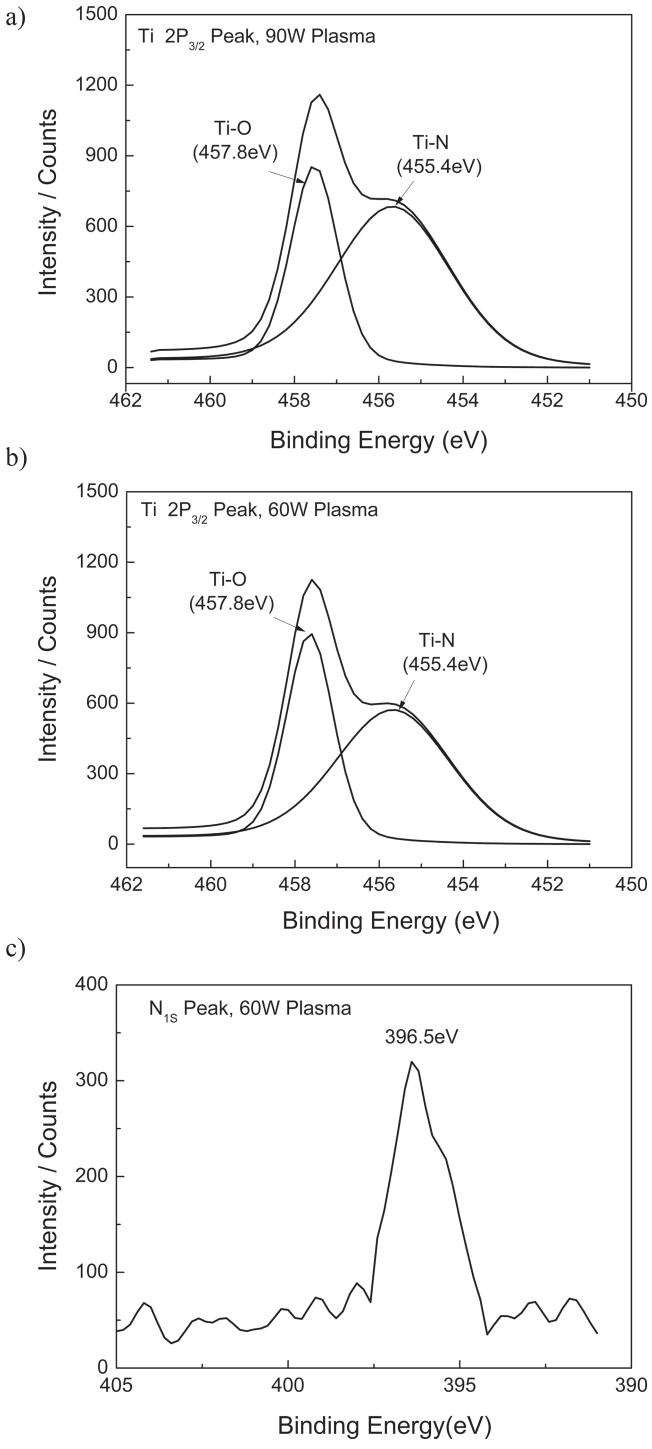

Figure 4. High-resolution XPS spectra of hybrid films obtained from 0.3 L/min N_2 flow rate and different plasma power a) Ti_{2p} peak with 90 W plasma power, b) Ti_{2p} peak with 60 W plasma power and c) N_{1s} peak with 60 W plasma power.

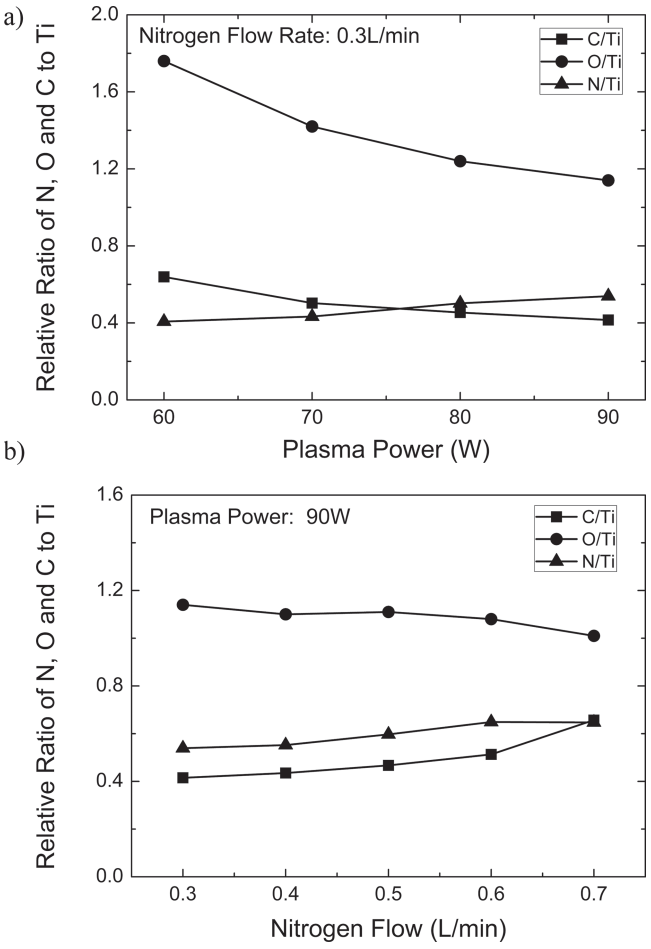

Figure 5. Plots of atomic ratios of C, O and N to Ti a) versus different plasma power b) versus different N_2 flow rate.

High-resolution X-ray photoelectron spectropy (XPS) Ti_{2p} and N_{1s} peaks of TiN_x/TiO_2 films deposited under the same 0.3 L/min N_2 flow rate but different plasma power levels are shown in **Figure 4**. The peak at a binding energy of 457.8 eV refers to the Ti_{2p} peak of TiO_2.[1] The shoulder peak for Ti_{2p} at 455.4 eV and the N_{1s} peak at 396.5 eV are consistent with nanocryatalline TiN_x thin films prepared using hydrothermal,[18] r.f. sputtering[19] or DC plasma methods.[20] With increasing plasma power, the TiN_x content of the hybrid film clearly increased as indicated by the increasing ratio of the TiN_x (455.4 eV) to TiO_2 (457.8 eV) peaks apparent with higher plasma power in the XPS spectra.

Using full XPS spectra, the total atomic ratios of carbon C, oxygen O and N to the total Ti content in the TiN_x/TiO_2 hybrid films deposited on PC were determined and are plotted as a function of plasma power and N_2 flow rate in **Figure 5**. At a fixed N_2 flow rate of 0.3 L/min, the N content of the hybrid films increased slightly with increasing plasma power indicating increased TiN_x formation (Figure 5a). The C content decreased marginally and the O content decreased markedly with increasing plasma power suggesting more decomposition of the precursor molecules with higher plasma power. The more efficient decomposition of the precursor together with the increased energy of the remaining excited nitrogen species are expected to favor the TiN_x formation reaction. At a fixed 90 W plasma power, the N content increased with N_2 flow rate until ~0.6 L/min where it saturated. The C content also

Table 1. Compositions of hybrid films before and after annealing.

Elements	Before Annealing	After Annealing
Ti	30.8%	34.6%
O	33.4%	35.0%
C	15.9%	4.3%
N	19.9%	26.1%

increased over the same range but increased more noticeably after 0.6 L/min. These two trends suggest that at ~0.6 L/min the available excited species related to the fixed plasma power are no longer able to effectively decompose the precursor and the TiN_x content stabilizes while the C content increased likely in the form of organic residue from the precursor. We note finally that over the full range of N_2 flow rates examined, the O content decreased slightly related to the decreased formation of TiO_2 and oxidized organic species when there is more N species present in the post-discharge region.

The C, O, N and Ti content in the hybrid films before and after annealing in N_2 are shown in **Table 1**. The C content decreased dramatically after annealing indicating that high temperature annealing is effective in reducing organic residues as previously reported.[21,22] During annealing, carbon is expected to be volatilized by oxidation with free oxygen in the films.[23,24] The increased TiO_2 and TiN_x crystallinity of the films after annealing was also noted above (Figure 3).

2.2. Film Properties

Optical transmittance spectra in the wavelength range of 420 to 800 nm for the TiN_x/TiO_2 films on PC substrates as a function of plasma power and N_2 flow rate are shown in **Figure 6**. The transmission spectrum for the PC substrate is included for comparison. With fixed 0.3 L/min N_2 flow rate during deposition, the average transmittance decreased over the entire visible wavelength range with increasing plasma power (Figure 6a). Increasing film thickness associated with increasing plasma power (Figure 2) resulted in lower transmittance. In addition, increasing TiN_x content with increasing plasma power also resulted in lower transmittance. The TiN_x phase is the main light absorbing phase of the hybrid film and was previously shown to increase with increasing plasma power (Figure 4a). Both film thickness and TiN_x content result in the decreased transmission observed. With a fixed plasma power of 90 W, the transmission spectra were observed to decrease with increasing N_2 flow rate as revealed in Figure 6b. The average transmittance decreased from 75% to 71% as N_2 flow rate increased from 0.3 L/min to 0.6 L/min. The decrease in optical transmittance was related to the two competing effects of film thickness and TiN_x content. With increasing N_2 flow rate the TiN_x content increased and the film thickness decreased resulting in the trend observed.

The electrical resistivity dependences of the films on plasma power and N_2 flow rate are shown in **Figure 7**. The resistivity before annealing exhibited a range from conductive (8.5×10^1 ohm cm) to near insulating properties (2.4×10^5 ohm

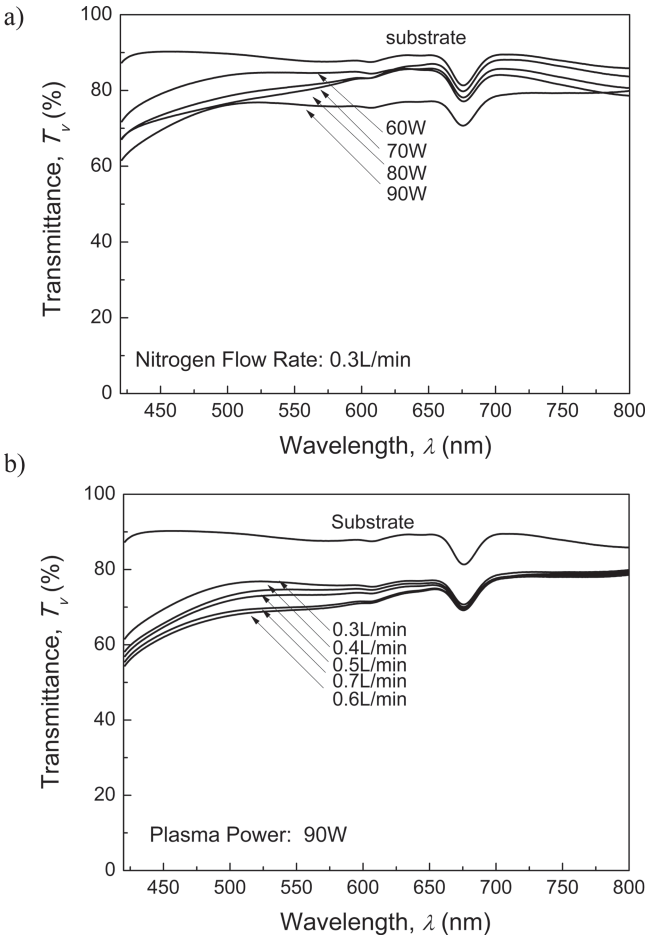

Figure 6. Transmittance spectra with wavelengths from 420 nm to 800 nm for a) different plasma power and b) different N_2 flow rate.

cm). Figure 7a shows that resistivity of the hybrid thin film decreased with the increasing plasma power. This trend is related to the increasing TiN_x content, which has a lower resistivity, with increasing plasma power as revealed by XPS analysis (Figure 5a). In addition, the carbon content of the hybrid film decreased with increasing plasma power, decreasing the resistivity related to the organic residues that reduce electron mobility.

The relationship between hybrid film resistivity with N_2 flow rate deposited at a constant plasma power of 90 W are shown in Figure 7b. As the N_2 flow rate increased from 0.3 L/min to 0.6 L/min, the film resistivity decreased. Two factors are expected to contribute to the result. First, as revealed by XPS, the TiN_x content increased with N_2 flow rate. Second, with higher N_2 flow rate, the reduced energy of the excited species and resulting reduced mobility of the dissociated precursor during film growth lead to more defect concentrations in the hybrid film which further reduced the resistivity. Increasing the N_2 flow rate above ~0.6 L.min lead to a dramatic increase in the film resistivity due to organic residues as revealed by XPS and noted previously (Figure 5b). Without annealing, the lowest resistivity (8.5×10^1 ohm cm) was achieved with 100 W plasma power and 0.6 L/min N_2 flow rate.

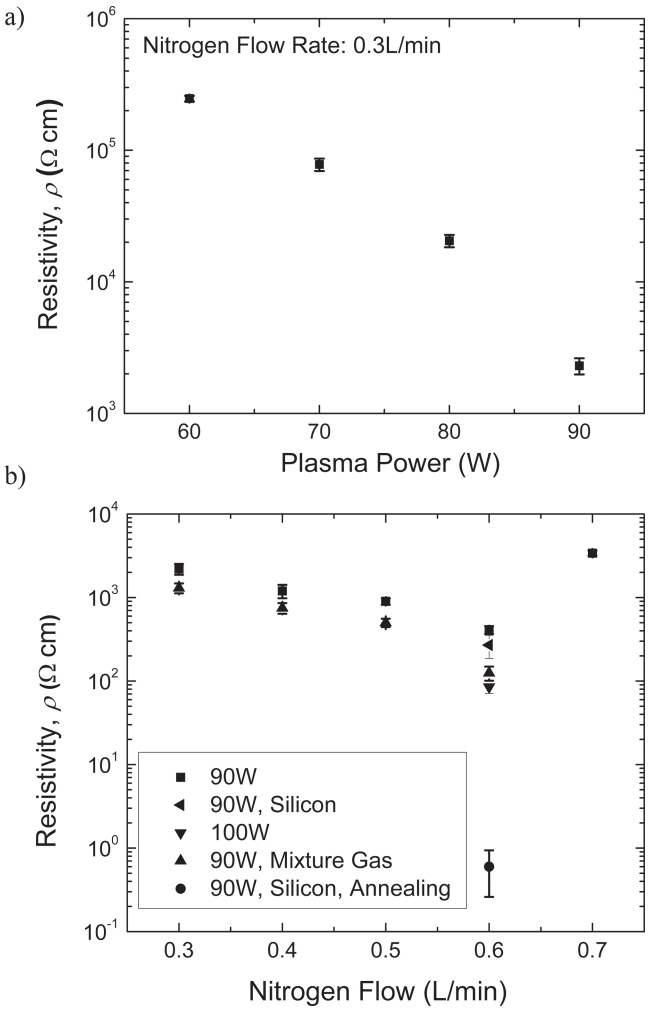

Figure 7. Variation of the resistivity of TiN_x/TiO_2 hybrid films influenced by a) plasma power b) N_2 flow, annealing and 2% H_2 mixture gas balanced by helium as plasma source.

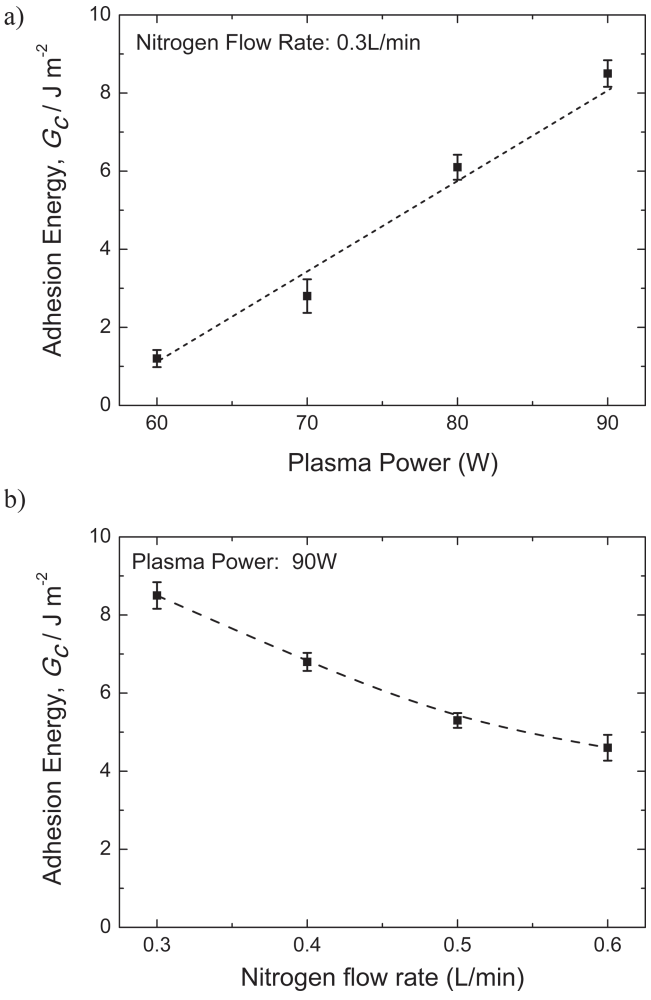

Figure 8. Variation of adhesion energy on PC substrate as a function of a) plasma power b) N_2 flow rate.

The effect of the 2% H_2 addition to the helium primary plasma gas on reducing the resistivity of the hybrid film is also shown in Figure 7b. The H_2 addition creates a reducing environment and also forms ammonia (NH_3) in the plasma region which is very effective at reducing organic residuals in the film.[25,26] Finally, the dramatic effect of annealing on the electrical resistivity of the film deposited at 90 W and 0.6 L/min from 2.7×10^2 ohm cm before annealing to 6.1×10^{-1} ohm cm after annealing is included in Figure 7b. As noted previously, the annealing results in increased conducting crystalline TiN_x phase and significantly reduced organic residuals. Clearly, while annealing of hybrid films on high melting point substrates may be an effective strategy to reduce resistivity, its application on lower melting temperature plastics is limited.

2.3. Adhesion

The variation of adhesion energy G_c of the hybrid films to PC substrates as a function of the plasma power and N_2 flow rate during deposition is shown in **Figure 8**. With increasing plasma power, the G_c increased from 1.2 J/m^2 to 8.5 J/m^2 (Figure 8a). The relatively low adhesion value of 1.2 J/m^2 result from weaker van der Waals dispersion interactions across the interface together with molecular interdigitation of the film with the substrate surface. With increasing plasma power, the increasingly energetic plasma may activate the PC surface producing reactive groups along with increasing interfacial roughness and increased molecular interdigitation. These effects can dramatically increase adhesion. We recently demonstrated the efficacy of such plasma exposure of PC substrates on increasing the adhesion of dense siloxane hybrid films deposited with a similar atmospheric plasma process.[27] Figure 8b shows decreasing adhesion energy with increasing N_2 flow rate under a fixed 90 W plasma power. The decreasing adhesion is consistent with the decreased amount of excited helium species and lower energy and shorter lifetime of the excited nitrogen species with increasing nitrogen flow noted in section 2.1. We therefore expect that the PC surface activation and roughening would decrease leading to the reduced adhesion values observed.

3. Conclusions

Transparent conductive TiN_x/TiO_2 hybrid films were successfully deposited by atmospheric plasma processing in ambient air on PC and silicon substrates using a titanium ethoxide precursor. The deposition rates ranged from ~125 to 150 nm/min. XRD and XPS results revealed that the composition of the hybrid films before annealing was amorphous and crystalline TiO_2 rutile phase and amorphous TiN_x. The visible transmittance of the films varied from 71 to 83% which decreased with increasing plasma power and N_2 flow rate. The film resistivity was in the range of ~10^1–10^5 ohm cm before annealing. Both annealing and introducing H_2 into the primary plasma were shown to be effective in reducing the resistivity. The adhesion energy of the hybrid films to the PC substrate was in the range ~1.2–8.5 J/m^2 depending on the plasma power and N_2 flow rate during deposition. Higher plasma power and lower N_2 flow rates were shown to improve adhesion values.

4. Experimental Section

Film Deposition: An atmospheric 13.56 MHz RF plasma source equipped with a scanning sample stage and a 25 mm dia. cylindrical plasma shower head (Atomflo 400D system, Surfx Technologies LLC, US) was employed. The flow rates of the primary and secondary plasma gas were controlled by the plasma system. The plasma was generated with a primary gas of 30 L/min of high purity compressed He (99.995%) and a secondary gas of N_2 (99.999%) with adjustable flow rates of 0.3 to 0.7 L/min. For some films, 2% H_2 was introduced into the Primary He gas. Titanium ethoxide (TTEO, 97%, Sigma-Aldrich) was used as the precursor, heated to 125 °C and then delivered to the flowing post-discharge plasma region by a high temperature precursor delivery system that is described in detail elsewhere.[12] High purity compressed He was also employed as the dilution and bubbler gas in the precursor delivery system with a flow rate of 1.0 L/min and 0.15 L/min, respectively. Reactive nitrogen species generated in the plasma region include ground-state atomic nitrogen N(^{4}S), which acts as the main reactant to form nitride, and three excited states of molecular nitrogen, including N_2 ($A^3\Sigma_u$), N_2 ($B^3\Sigma_g$), and N_2 ($C^3\Sigma_u$).[28]

Polycarbonate with 70 × 10 × 6.5 mm^3 dimensions (PC, Makrolon® GP, Bayer Material Science AG, Germany) and standard silicon wafer with 15 × 15 × 0.78 mm^3 dimensions were used as substrates. The substrates were degreased by isopropanol for cleaning before deposition. The distance between the plasma source and the substrate surface was set to 1.0 mm. The films were deposited in single pass at a scan velocity of 10 mm/s and step size of 0.3 mm. In order to investigate the effect of plasma power and nitrogen flow rate, TiN_x/TiO_2 hybrid films were deposited onto PC substrates with various plasma power conditions (60–100 W) and different N_2 flow rates (0.3–0.7 L/min). The deposition conditions are summarized in **Table 2**. The TiN_x/TiO_2 thin films were also deposited on Si substrate to allow the investigation of annealing at elevated temperature. The annealing was conducted in an oven (Yield Engineering Systems, Inc., US) for 4 hours in N_2 at a temperature of 400 °C.

Film Characterization: A surface profilometer (Veeco Dektak 150, Veeco Instruments Inc., US) was used to measure the film thickness on the PC substrate with a film edge created by masking a small region. A UV-Vis-NIR spectrophotometer (Cary 6000i, Agilent Technologies Inc., US) was employed to test the visible transmittance of the films. The average transmittance was calculated by averaging the values obtained for the wavelength in the range of 420 to 800 nm. X-ray Photoelectron Spectroscopy (XPS, PHI 5000 Versaprobe, Physical Electronics Inc., US) was applied to evaluate the composition of the film. An Al–K_α (1486 eV) X-ray source with a spot size of ~1 mm was equipped (pass energy 117.4 eV, scan range 0–1000 eV and 1 eV/step). Prior to the measurement, surface atmospheric contaminants were removed by ion sputtering for 2 min. Argon ion beam was applied to sputter off the hybrid thin film, with the setting of 1 kV, 0.5 μA, and 2 mm × 2 mm sputter spot. The angle between the detector and the sample surface was 45°. High resolution scan was also employed for achieving information of Ti_{2p} and N_{1s} peak (pass energy 23.5 eV, scan range 20 eV and 0.2 eV/step). A Software was used for peak analysis after high resolution scan. Scanning electron microscopy (Sirion XL30, FEI Co. Ltd., US) was used to examine the microstructure of the films on the surface. X-Ray Diffraction spectrum was determined using X'Pert Materials Research Diffractometer (PANalytical, Inc, Netherland) with Cu Kα radiation operating at 45 kV. The sample was mounted on a vertical sample stage. Data were collected using a step width of 0.01° and step time of 0.1 s with a 2θ range from 25.0° to 60.0°. A four-point probe devise (200 mm Probe Station, Cascade Microtech, Inc., US) with a semiconductor parameter analyzer (4156C, Agilent Technology, Inc., US) was carried out to investigate the resistivity of the samples. The resistivity of the hybrid film was calculated using van der Paul method.[29] The resistivity is given by the following equation:

$$\rho = k \times \frac{V}{I} \times t \tag{1}$$

Where k is a constant and equals approximately to 4.53.[30] Value of V/I is the slope of plot obtained by four point probe measurements and t is the thickness of hybrid film.

Adhesion Measurement: The adhesion energies, G_c, of the TiN_x/TiO_2 hybrid films on the polycarbonate substrates were measured using a double cantilever beam (DCB) specimen. Details of the DCB techniques can be found elsewhere.[31,32] Test specimens were prepared by bonding an identical blank PC beam onto the hybrid film deposited on an underlying PC substrate using a thin epoxy layer (<2 μm). The specimen was mounted into an adhesion testing system (Delaminator, DTS company, US) with metal loading tabs glued on two sides of the specimen. The initial crack was introduced from the edge of the sample by applying a tensile load. The specimen was loaded in tension with a displacement rate of 1.0 μm/s until the crack extension and then unloaded. The fracture energy, G_c was calculated by the following equation:[33]

$$G_c = \frac{12P_c^2a^2}{B^2E'h^3}\left(1+0.64\frac{h}{a}\right)^2 \tag{2}$$

Table 2. Deposition conditions.

Parameter	Unit	Conditions
Primary gas		He (99.995%)
		2% H_2 He Mixture gas
Secondary gas		N_2 (99.995%)
Bubbler and dilution gas		He (99.995%)
Primary gas flow	L/min	30
Secondary gas flow	L/min	0.3, 0.4, 0.5, 0.6, 0.7
Bubbler gas flow	L/min	0.15
Dilution gas flow	L/min	1.0
Plasma power	W	60, 70, 80, 90, 100
Deposition distance	mm	1.0
Gun move velocity	mm/s	10
Step	mm	0.1
Number of pass		1

In this equation, P_c is the critical load at which crack growth occurs, a is the corresponding crack length, E' is the plain strain elastic modulus of the substrate, and B and h are the width and thickness of the substrate. The crack length a was obtained from the compliance of the unloading curve.[33] This procedure was continued until the crack length became the length of $(L\text{-}4\ h)$, where L is the length of the substrate. All tests were conducted in a laboratory air environment at room temperature.

Acknowledgements

The authors would like to thank the US Department of Energy for their financial support under Contract No. DE-FG02–07ER46391.

Received: August 30, 2013
Revised: December 4, 2013
Published online: January 28, 2014

[1] S. Shimada, M. Yoshimatsu, H. Nagai, M. Suzuki, H. Komaki, *Thin Solid Films* **2000**, *370*, 137–145.
[2] G. Zhao, T. Zhang, T. Zhang, J. Wang, G. Han, *J. Non-Cryst. Solids* **2008**, *354*, 1272–1275.
[3] B. H. Weiller, *J. Am. Chem. Soc.* **1996**, *118*, 4975–4983.
[4] S. Shimada, Y. Takada, J. Tsujino, *Surf. Coatings Technol.* **2005**, *199*, 72–76.
[5] A. Weber, R. Nikulski, C. P. Klages, *Appl. Phys. Lett.* **1993**, *63*, 325.
[6] J. Wu, R. I. Murakami, M. Kondo, *Int. J. Modern Phys. B* **2003**, *17*, 1177–1182.
[7] Z. Cheng, H. Peng, G. Xie, Y. Shi, *Surf. Coatings Technol.* **2001**, *138*, 237–241.
[8] H. Li, W. Pan, W. Zhang, S. Huang, H. Wu, *Adv. Funct. Mater.* **2013**, *23*, 209–214.
[9] K. Sieradzka, M. Mazur, D. Wojcieszak, J. Domaradzki, D. Kaczmarek, E. Prociow, *Thin Solid Films* **2012**, *520*, 3472–3476.
[10] W. Shimizu, S. Nakamura, T. Sato, Y. Murakami, *Langmuir* **2012**, *28*, 12245–12255.
[11] C. K. Chung, M. W. Liao, C. W. Lai, *Thin Solid Films* **2009**, *518*, 1415–1418.
[12] L. Cui, A. N. Ranade, M. A. Matos, L. S. Pingree, T. J. Frot, G. Dubois, R. H. Dauskardt, *ACS Appl. Mater. Interfaces* **2012**, *4*, 6587–6598.
[13] D. Pappas, *J. Vacuum Sci. Technol. A* **2011**, *29*, 020801.
[14] J. H. Lee, Y. S. Kim, J. S. Oh, S. J. Kyung, J. T. Lim, G. Y. Yeom, *J. Electrochem. Soc.* **2009**, *156*, 248–252.
[15] S. Kang, S. Jeong, K. Kwon, K. Park, *J. Nanosci. Nanotechnol.* **2013**, *13*, 8101–8105.
[16] D. Merche, N. Vandencasteele, F. Reniers, *Thin Solid Films* **2012**, *520*, 4219–4236.
[17] A. Tarniowy, R. Mania, M. Rekas, *Thin Solid Films* **1997**, *311*, 93–100.
[18] M. Wu, *J. Alloys Compounds* **2009**, *486*, 223–226.
[19] B. Yoo, K.-J. Kim, Y. H. Kim, K. Kim, M. J. Ko, W. M. Kim, N.-G. Park, *J. Mater. Chem.* **2011**, *21*, 3077.
[20] E. Galvanetto, F. P. Galliano, F. Borgioli, U. Bardi, A. Lavacchi, *Thin Solid Films* **2001**, *384*, 223–229.
[21] J. G. Korvink, P. J. Smith, D. Y. Shin, Inkjet-Based Manufacturing, Wiley-VCH, Weinheim, Germany **2012**.
[22] K. Kumar, Y. Kim, E. Yang, *Carbon* **2013**, *65*, 35–45.
[23] R. Yang, C. Chu, Y. Peng, H. Chueng, *Adv. Mater. Sci. Engin.* **2012**, Article ID 741561.
[24] S. Sung, M. S. Park, D. Kim, J. Kang, *Bull. Korean Chem. Soc.* **2013**, *34*, 1473.
[25] R. M. Fix, R. G. Gordon, D. M. Hoffman, *J. Am. Chem. Soc.* **1990**, *112*, 7833–7835.
[26] J. A. Prybyla, C. M. Chiang, L. H. Dubois, *J. Electrochem. Soc.* **1993**, *140*, 2695–2702.
[27] L. Cui, A. N. Ranade, M. A. Matos, G. Dubois, R. H. Dauskardt, *ACS Appl. Mater. Interfaces* **2013**, *5*, 8495–8504.
[28] G. R. Nowling, S. E. Babayan, V. Jankovic, R. F. Hicks, *Plasma Sources Sci. Technol.* **2002**, *11*, 97–103.
[29] L. Massissel, R. Glang, *Handbook of Thin Solid Films Technology*, McGraw-Hill Book Company, New York **1970**.
[30] M. F. Smits, *Bell Lab Tech. J.* **1958**, *37*, 711–718.
[31] R. H. Dauskardt, M. Lane, Q. Ma, N. Krishna, *Engin. Fracture Mech.* **1998**, *61*, 141–162.
[32] Y. Matsuda, S. W. King, J. Bielefeld, J. Xu, R. H. Dauskardt, *Acta Materialia* **2012**, *60*, 682–691.
[33] M. F. Kanninen, *Int. J. Fracture* **1973**, *9*, 83–92.